ELSEVIER

Biophysical Chemistry 91 (2001) 305–317

Biophysical Chemistry

www.elsevier.com/locate/bpc

Homology modeling of wild type and pyrimethamine/cycloguanil-cross resistant mutant type *Plasmodium falciparum* dihydrofolate reductase. A model for antimalarial chemotherapy resistance

Osvaldo Andrade Santos-Filho[a,1], Ricardo Bicca de Alencastro[b], Jose Daniel Figueroa-Villar[a,*]

[a] *Departamento de Química, Instituto Militar de Engenharia, Praça General Tibúrcio 80, Praia Vermelha 22290-270, Rio de Janeiro, Brazil*

[b] *Physical Organic Chemistry Group, Departmento de Química Orgânica, Instituto de Química, Universidade Federal do Rio de Janeiro, Ilha do Fundao, CT, Bloco A, Lab. 609, 21949-900 Rio de Janeiro, Brazil*

Received 20 March 2001; received in revised form 30 May 2001; accepted 31 May 2001

Abstract

We propose a low-resolution model for both the wild type and the pyrimethamine (Pyr)/cycloguanil (Cyc) cross-resistant mutant type *Plasmodium falciparum* DHFR (*Pf* DHFR), based on homology modeling using chicken liver DHFR as a template. The built models contain five α-helices, eight β-sheets, eight tight turns and several loops. The Ramachandran plot for the models shows 95.3 and 100% of the amino acid residues in the favorable regions for the whole enzymes and for the active sites, respectively. Furthermore, we made a preliminary analysis of the complexes Pyr/Cyc-wild DHFR and Pyr/Cyc-mutant DHFR in order to explain the probable mechanism of resistance. Our results show that the steric factor may be the main structural cause of *P. falciparum* resistance toward antifolate drugs. © 2001 Published by Elsevier Science B.V.

Keywords: Malaria; Homology modeling; *Plasmodium falciparum*; Dihydrofolate reductase; Chemotherapy; Resistance

* Corresponding author. Tel.: +55-21-546-7057; fax: +55-21-546-7059.

E-mail address: d5figuer@epq.ime.eb.br (J. Daniel Figueroa-Villar).

Received 20 March 2001; received in revised form 30 May 2001; accepted 31 May 2001

[1] Current address: Physical Organic Chemistry Group, Departamento de Qumica Organica, Instituto de Qumica, Universidade Federal do Rio de Janeiro, Ilha do Fundao, CT, Bloco A, Lab. 609, 21949–900, Rio de Janeiro, Brazil.

0301-4622/01/$ - see front matter
PII: S0301-4622(01)00180-6

1. Introduction

In spite of early progress, malaria is still one of the most serious health problems facing humanity. It affects 300–500 million people causing over 2.5 million deaths annually, mostly in children. Today, the threat is more significant for nations in Latin America, Africa, Asia and in some regions of the South Pacific, but, in all, approximately 40% of the world population risk catching malaria [1]. This disease is caused by protozoan parasites of the genus *Plasmodium*. In humans, four species are responsible for malaria: *P. falciparum; P. vivax; P. ovale;* and *P. malariae*. The first one is the most dangerous. Two aspects have currently stimulated new efforts regarding medical and molecular studies about malaria: the rapid emergence of *P. falciparum* strains resistant to currently available antimalarial drugs [2–5]; and the inefficacy of malarial vaccines [6].

Many strategies are used in developing antimalarial chemotherapy. One of them involves the use of dihydrofolate reductase inhibitors as potential antimalarial drugs. Dihydrofolate reductase [DHFR, 5,6,7,8-tetrahydrofolate-$NADP^+$ oxidoreductase (E.C. 1.5.1.3)] is the enzyme that catalyses the NADPH-dependent reduction of 7,8-dihydrofolate to 5,6,7,8-tetrahydrofolate, which is the precursor of the co-factors required for the synthesis of purine nucleotides, thymidylate and several amino acids [7]. Thus, inhibition of DHFR can lead to the disruption of DNA synthesis and the death of the rapidly proliferating cells [7,8]. This enzyme has been successfully used as a good target for the treatment of cancer, bacterial infections and malaria. A vast amount of information about DHFR has been published and reviewed [7–10].

Pf DHFR exists as a domain of a bifunctional enzyme, DHFR-thymidylate synthase (TS, 5,10-methylenetetrahydrofolate: dUMP C-methyltransferase, E.C. 2.1.1.45), linked to the TS domain by a junctional sequence of 94 amino acids [11]. The DHFR domain of the enzyme includes 228 residues (residues 1-228), and the TS domain includes 286 residues (residues 323–608). There is evidence that the DHFR of other protozoa is similarly bifuncional [7].

Pyr and Cyc are potent inhibitors of *Pf* DHFR, acting by selective inhibition of malarial DHFR. However, the rapid emergence of antifolate resistant malaria has compromised the clinical utility of these drugs. Analysis of the DHFR sequences of several Pyr- and Cyc-resistant *P. falciparum* strains revealed correlation between antifolate resistance and point mutations of the DHFR gene. Mutations in *Pf* DHFR involving amino acid residues 16, 51, 59, 108 and 164 have been reported [12–19]. Ser-108 → Asn-108 is a critical point mutation found in all Pyr-resistant strains, and it is believed to be the prime point mutation necessary for the development of malarial resistant mutants to antifolates. The Ala-16 → Val-16 mutation confers resistance only to Cyc, and is always found to be associated with the Ser-108 → Asn-108 mutation [17]. Also the Ile-164 → Leu-164 mutation, in combination with the Ser-108 → Asn-108 mutation and one or both of the Asn-51 → Ile-51 or Cys-59 → Arg-59 mutations, has been found in *P. falciparum* strains that are highly resistant to both drugs, Pyr and Cyc [17,19].

Structure-based approaches using the target 'receptor' structure are helpful in designing lead compounds and in developing more selective drugs. However, up to this moment, the crystallographic structure of *Pf* DHFR has not been obtained. In order to address the problem of binding modes for some antimalarial drugs on *Pf* DHFR, two homology models for the malarial enzyme have recently appeared in the literature [20,21]. The *Pf* DHFR homology-model proposed by Lemcke and co-workers [20] was obtained by amino acid substitution in human DHFR [22]. Based on this model, the investigators confirmed the hypothesis regarding the Ser-108 → Asn-108 point mutation in relation to Pyr resistance. However, the authors were not able to explain the enhanced resistance caused by the Asn-51 → Ile-51 and Cys-59 → Arg-59 mutations. Rastelli et al. [21], have built wild-type and Ala-16 → Val-16, Ser-108 → Thr-108 and Ala-16 → Val-16 + Ser-108 → Thr-108 mutant-types *Pf* DHFR homology-models. Their models were based on multiple sequence alignment among the amino acid sequence of *Pf* DHFR [11] and the amino acid sequences of the crystal structures of DHFRs

from *Escherichia coli* [23], *Lactobacillus casei* [24], human [22], chicken liver [25] and *Pneumocystis carinii* [26]. These authors suggested explanations for the Cyc resistance and Pyr susceptibility in relation to the Ala-16 → Val-16 mutation of the *Pf* DHFR domain.

In this work, we propose *Pf* DHFR homology-models for both the wild-type (Ser-108), and Pyr and Cys cross-resistant mutation-type *Pf* DHFR (Asn-51 → Ile-51, Cys-59 → Arg-59, Ser-108 → Asn-108, Ile-164 → Leu-164 mutations) based on the chicken liver DHFR crystallographic structure [25]. Our models were submitted to a validation process that showed them to be satisfactory. The results were satisfactory regarding stereochemical and structural parameters. The *Pf* DHFR-drug complexes were generated by docking each of the drugs, Pyr and Cyc, to the enzyme. Molecular dynamics simulations were done on the complexes in order to obtain information about the binding process and the provable resistance mechanism. The comparison between the complexes was carried out by the superposition of the main amino acid residues at the active sites.

2. Experimental

The sequence of the *Pf* DHFR used was the one determined by Bzik and co-workers [11]. The amino acid sequences of human DHFR (PDB entry *1dhf*) [22], *E. coli* DHFR (PDB entry *1ra9*) [23] and chicken liver DHFR (PDB entry *8dfr*) [25], taken from the protein data bank (PDB) [27,28], were used as potential templates. The sequences were then aligned using the Multalign program [29]. Thus, we were able to choose, among the three crystallographic structures, the one that works better as the main template for the generation of the desired homology-model. As described in Section 3, the chosen template was chicken liver DHFR. We used the Swiss-PdbViewer program [30] to align the sequences of *P. falciparum* and chicken liver DHFRs. Then, this alignment was submitted to the SWISS-MODEL server [30–32] to generate an initial model. After obtaining the model, we made some adjustments on the original alignment, followed by a resubmission to the SWISS-MODEL server. The obtained model was then submitted to energetic and structural loop refinement, using the database for loops as implemented in the Swiss-PdbViewer program [30]. After the docking of the co-factor into the active site of the modeled *Pf* DHFR, we carried out some energy optimizations using molecular mechanics calculations. In order to generate the mutant-type *Pf* DHFR, we did specific point mutations (Asn-51 → Ile-51, Cys-59 → Arg-59, Ser-108 → Asn-108, and Ile-164 → Leu-164) on the wild-type modeled enzyme, followed by minimization procedures. The validation of the generated homology-models was done with the PRO CHECK [33] and WHAT IF [34] programs, available at Biotech Validation Suite for Protein Structures [35]. In order to study the interaction features between both the wild- and mutant-type *Pf* DHFR and the drugs Pyr and Cyc, docking of both drugs into the active site of each enzyme was carried out, followed by molecular dynamics simulations.

The hardware resources used in this work were a workstation Silicon Graphics IRIX O2 6.3, and a PC Pentium II.

3. Results and discussion

3.1. Homology modeling of Plasmodium falciparum DHFR

As a first step, the primary structure of the *P. falciparum* DHFR [11] was analyzed. This analysis showed that the amino acid sequence has an Asn residue at position 108. This single point mutation on codon 108 from Ser to Asn on chromosome 4 has been identified as the major change underlying resistance to pyrimethamine [2,36–39]. Thus, in order to obtain the model for the wild-type *Pf* DHFR, a preliminary Asn-108 → Ser-108 mutation was done in the *Pf* DHFR amino acid sequence. Then, this sequence and the sequences of DHFRs from human [22], *E. coli* [23] and chicken liver [25], were aligned using the Multalign program [29]. The results showed that the *Pf* DHFR sequence has 35.43, 34.09 and 32.69% identity degree with the chicken liver, the human

and the *E. coli* DHFRs, respectively. Consequently, we decided to use the chicken liver DHFR as the main template during the homology-modeling of the *Pf* DHFR.

The next step was to do a single alignment between the amino acid sequences of the target enzyme (*Pf* DHFR) and the template enzyme (chicken liver DHFR), as shown in Fig. 1. This was accomplished by using the facilities of the Swiss-PdbViewer program [30]. Then, this alignment was submitted to the SWISS-MODEL server [30–32] to generate an initial model. The alignment automatically generated was inspected by comparison with the three-dimensional structure of the template enzyme. As may be observed in bold character in Fig. 1, this alignment shows two unsuitable discontinuities on the amino acid residues from *Pf* DHFR, spanning from Glu-71 (E71) to Lys-74 (K74) and from Cys-78 (C78) to Asn-82 (N82). It was noticed that such discontinuities resulted in a considerable distortion of the modeled enzyme. To overcome this problem, we altered the alignment by moving the residues Lys-32 (K32), Tyr-33 (Y33), Phe-34 (F34), Gln-35 (Q35) and Arg-36 (R36) of the chicken liver DHFR from their original positions to the position adjacent to residue Tyr-31 (Y31). This new alignment, shown in Fig. 2, was resubmitted to the SWISS-MODEL server, and the results were checked again. The loops on the *Pf* DHFR were modeled using a structural database for loops from other proteins with the same sequence length and similar anchor residues, which is available on the Swiss-PdbViewer program [30].

The whole model of the generated *Pf* DHFR was next minimized with the AMBER force field [40–42], implemented in the Insight II 97.0/Discover package [43], using the steepest descent and conjugate gradient algorithms [44,45]. At this stage, our goal was to relax the modeled system and to arrive at a better conformation, which would be reflected in a good Ramachandran plot [46]. To accomplish that, we conducted several tests varying the convergence criterion and found that 10.00 kcal mol^{-1} $Å^{-1}$ gave the best results when using the distance-dependent dielectric constant of water ($\varepsilon_r = 78.54$) during the minimization.

The main structural elements of the optimized *Pf* DHFR homology-model are shown in Fig. 3. The model is formed by eight strand-twisted β-sheets, composed of seven parallels and one antiparallel strand. The remainder of the enzyme comprises five α-helices, eight tight turns and several extended loops. It is interesting to mention that, as in the case of both human and chicken liver DHFRs [22,25], disruptions are few within some β-sheets. As a result, these sheets

```
Plasmodium   1   MMEQVCDVFD IYAICACCKV ESKNEGKKNE VFNNYTFRGL GNKGVLPWKC
18DFR        1       VRSLNS IVAVCQNM-- ---------- --------GI GKDGNLPWP-
                     *  .   ***.*                          *. *. * ***
Plasmodium  51   NSLDMKYFCA VTTYVNESKY EKLKYKRCKY LNKETVDNVN DMPNSKKLQN
18DFR       26   -PLRNEY--- --------KY ----FQR--- --MTSTSHVE GK------QN
                   *   *             **      . *      . .  .*.  .       **
Plasmodium 101   VVVMGRTNWE SIPKKFKPLS NRINVILSRT LKEEDFDEDV YIINKVEDLI
18DFR       49   AVIMGKKTWF SIPEKNRPLK DRINIVLSRE LKEAP-KGAH YLSKSLDDAL
                  *.**.  *  *** * .**  .***..***  ***        *. . ..* .
Plasmodium 151   VLLG----KL NYYKCFIIGG SVVYQEFLEK KLIKKIYFTR INSTYECDVF
18DFR       98   ALLDSPELKS KVDMVWIVGG TAVYKAAMEK PINHRLFVTR ILHEFESDTF
                   **        .  .  *.** . **    .**   .  ... ** *   .* * *
Plasmodium 197   FPEINENEYQ IIS-----VS DVYTSNNTTL DFIIYKK
18DFR      148   FPEIDYKDFK LLTEYPGVPA DIQEEDGIQY KFEVYQKSV
                 ****......          . *.   .      * .* *
```

Fig. 1. Alignment between *Pf* DHFR and chicken liver DHFR (18DFR) (ExPDB database entry 18DFR, corresponding to PDB entry 8DFR, chicken liver DHFR). Identical residues are shown with stars, whereas residues with similar properties are shown with dots.

```
Plasmodium   1   MMEQVCDVFD IYAICACCKV ESKNEGKKNE VFNNYTFRGL GNKGVLPWKC
18DFR        1       VRSLNS IVAVCQNM-- ---------- --------GI GKDGNLPWP-
                      *  .   ***.*                          *. *. * ***
Plasmodium  51   NSLDMKYFCA VTTYVNESKY EKLKYKRCKY LNKETVDNVN DMPNSKKLQN
18DFR       26   -PLRNEYKYFQR--------- ---------- --MTSTSHVE GK------QN
                   *   *                          . .  .*.  .       **
Plasmodium 101   VVVMGRTNWE SIPKKFKPLS NRINVILSRT LKEEDFDEDV YIINKVEDLI
18DFR       49   AVIMGKKTWF SIPEKNRPLK DRINIVLSRE LKEAP-KGAH YLSKSLDDAL
                  *.**.  *  *** * .**  .***..***  ***         *. . ..* .
Plasmodium 151   VLLG----KL NYYKCFIIGG SVVYQEFLEK KLIKKIYFTR INSTYECDVF
18DFR       98   ALLDSPELKS KVDMVWIVGG TAVYKAAMEK PINHRLFVTR ILHEFESDTF
                  **        .  .  *.** . **   .**  .  ... ** *   .* * *
Plasmodium 197   FPEINENEYQ IIS-----VS DVYTSNNTTL DFIIYKK
18DFR      148   FPEIDYKDFK LLTEYPGVPA DIQEEDGIQY KFEVYQKSV
                  ****......          . *.   .      * .* *
```

Fig. 2. Modified alignment between *Pf* DHFR and chicken liver DHFR.

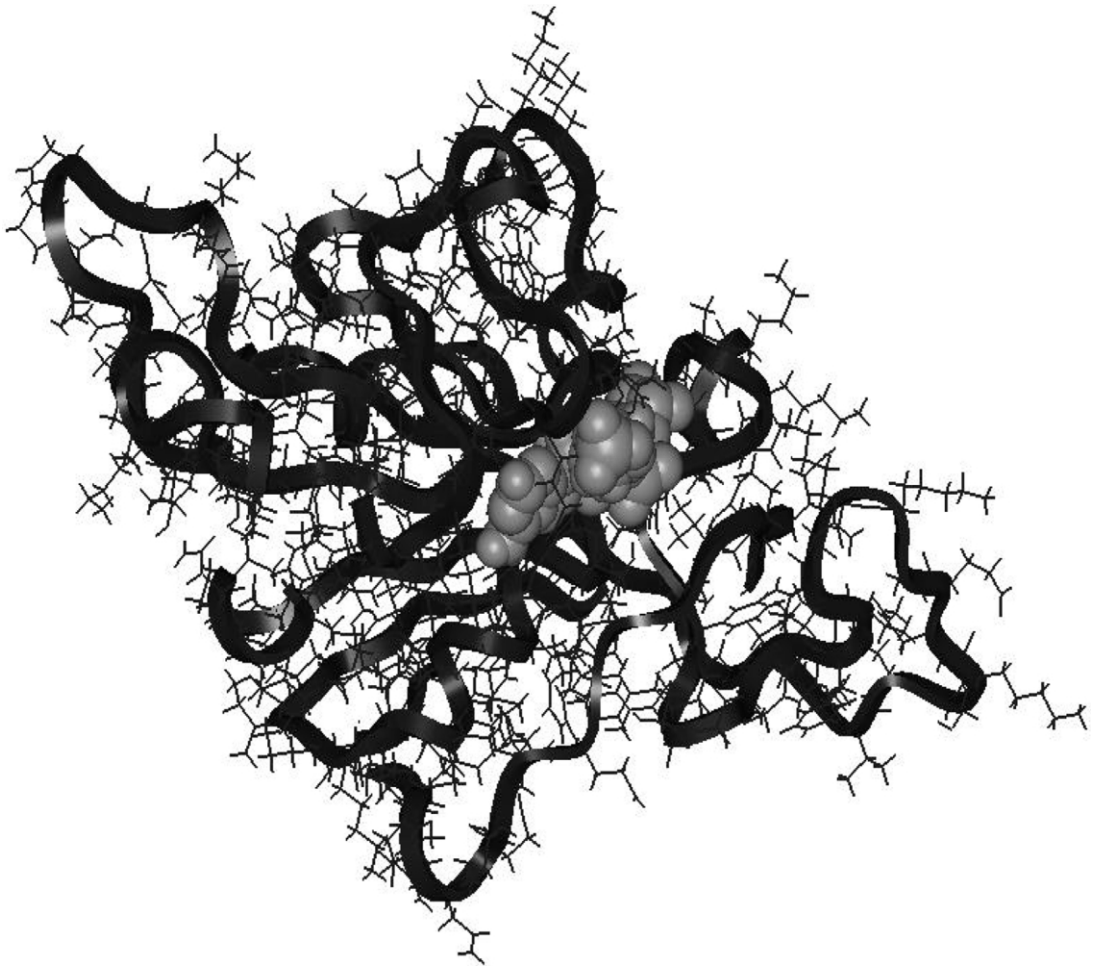

Fig. 3. Proposed wild-type *Pf* DHFR structure. NADPH is shown in gray.

are not continuous, but consist of two consecutive strands. These extended beta bulges, which are termed 'beta blow-out', were first noted by Volz et al. [47].

The above homology-modeled system is the *Pf* DHFR apoenzyme. In order to build the corresponding holoenzyme, we docked the co-factor, NADPH, into the active site of the modeled apoenzyme based on the chicken liver DHFR holoenzyme (PDB entry *8dfr*). Then, we minimized the NADPH using the CVFF force field [48–54] implemented in the Insight II 97.0/Discover package [43]. Such a minimization was done by successive optimizations with the following convergence criteria: 10.00; 1.00; 0.01; and 0.001 kcal mol^{-1} $Å^{-1}$ with steepest descent, conjugate gradient, quasi-Newton–Raphson and Newton–Raphson algorithms, respectively. Then, we optimized the whole holoenzyme until a 10.00-kcal mol^{-1} $Å^{-1}$ gradient was found (Fig. 3). As in the modeling of the apoenzyme, the distance-dependent water dielectric constant was used during the calculations.

In order to check the compatibility between the *Pf* DHFR homology-model and the three-dimensional structure of the used template (chicken liver DHFR), both of the enzymes were superimposed. The root-mean-square (RMS) deviation between them is 0.16 Å. This result shows that the modeled enzyme is satisfactory with regard to the utilization of the template enzyme during the homology-modeling process.

As mentioned above, we are interested not only in the wild-type, but also in the Pyr and Cyc cross-resistant mutant enzyme. Thus, some specific mutations (Asn-51 → Ile-51, Cys-59 → Arg-59, Ser-108 → Asn-108 and Ile-164 → Leu-164) were introduced on the wild-type modeled enzyme. Then, the mutant model was minimized, following the same procedure and criteria described for the wild enzyme.

3.2. Validation of the models

In order to check the quality of both the proposed wild-type and the mutant-type *Pf* DHFRs, each of them was submitted to validation analysis, using the PRO CHECK [33] and WHAT IF [34] programs. It is important to note that since only four amino acid residues (from a total of 228 residues) were changed in the wild-type enzyme to generate the mutant-type enzyme, the validation results found for both enzymes were approximately the same.

Fig. 4 is the Ramachandran plot [46] of the *Pf* DHFR, generated with the PRO CHECK program [33]. Glycine residues are separately identified by triangles. The shading represents the different regions of the plot, the darker the area the more favorable the ϕ-ψ combination. According to that plot, 95.3% of the amino acid residues of the *Pf* DHFR proposed model are in favorable regions of the plot.

Regarding the main-chain properties of the modeled enzyme, no considerable bad contacts, nor C_α tetrahedron distortion nor hydrogen-bond energy problems were found. Moreover, the average G-factor [33], the measure of the normality degree of the protein's properties, is inside permitted values. Also no distortions of the side-chain torsion angles were found.

It was noticed that just 31 out of a total of 228 amino acid residues (approx. 13.6% residues) show any geometric distortion. Both residues Met-1 and Val-151 have length bond deviations higher than 0.05 Å. Bend angle deviations were found for Thr-36, Phe-37, Arg-38, Leu-98, Gln-99, Asp-137, Glu-138, Val-152 and Leu-152. Small aromatic ring planarity deviations were found for 11 Tyr, 7 Phe and 2 Trp residues.

3.3. Active site determination

The active site of the *Pf* DHFR homology-model was determined based on the superposition of the modeled *P. falciparum*, the human (entry *1dhf*) [22] the *E. coli* (entry *1ra9*) [23] and the chicken liver (entry *8dfr*) [25] DHFRs. From the *E. coli* DHFR we selected those residues that interact with both NADPH and folate [23], residues that form the active site as suggested by Blaney and collaborators [55] and those residues that interact with Pyr [56]. From the chicken liver DHFR [25], were selected those residues that form its active site according to Blaney and Kraut [25,55,57,58]. From the human DHFR were se-

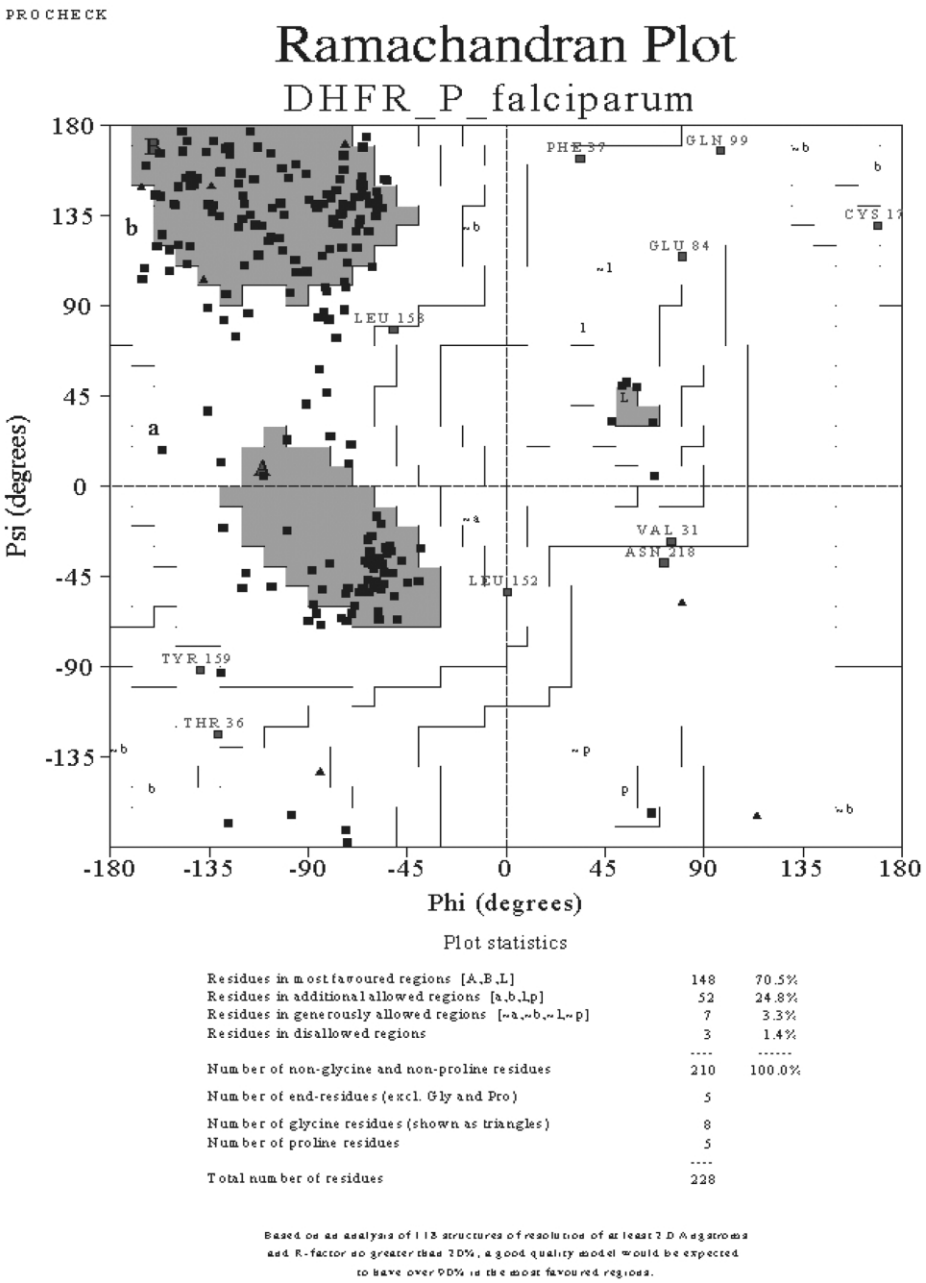

Fig. 4. Ramachandran plot of the proposed *Pf* DHFR homology-model.

lected those residues that form both the folate and the NADPH binding sites [22,59]. Thus, we obtained an 'amplified binding site' for the *Pf* DHFR homology-model constituted by 78 residues: Phe-9, Asp-10, Ile-11, **Ile-14**, **Ala-16**, Leu-40, Gly-41, Asn-42, Lys-43, Gly-44, Val-45, Leu-46, Pro-47, Trp-48, Lys-49, Cys-50, **Asn-51**, Ser-52, Leu-53, **Asp-54**, Met-55, Lys-56, Tyr-57,

Phe-58, **Cys-59**, Glu-71, Lys-72, Leu-73, Lys-74, Tyr-75, Lys-76, Arg-77, Asn-100, Val-101, Val-102, Val-103, Met-104, Gly-105, Arg-106, Thr-107, **Ser-108**, Trp-109, Ile-112, Pro-113, Lys-114, Lys-115, Phe-116, Lys-117, Pro-118, Leu-119, Ser-120, Asn-121, Arg-122, Ile-123, Asn-124, Ser-128, Arg-129, Thr-130, Lys-132, Ile-143, Lys-145, Val-146, **Ile-164**, Val-168, Val-169, Tyr-170, Gln-171, Glu-172, Phe-173, Leu-174, Glu-175, Lys-176, **Thr-185**, Thr-189, Arg-190, Ile-191, Asp-198 and Val-199.

Attention should be paid to the fact that all the residues that suffer mutations (Asn-51, Cys-59, Ser-108 and Ile-164), as well as those that form the antifolate binding site [60,61], shown in bold, are included into the 'amplified binding site'.

It was observed that the structural parameters of the majority of the 'amplified binding site' residues are in statistically favorable regions. The exceptions were Ile-11, which shows some minor χ_1 and χ_2 rotamer problems, Tyr-75, Trp-109, Tyr-170 and Phe-173, all of which show slight aromatic ring planarity deviations. Thus, we can conclude that 92.31% of the 'amplified binding site' *Pf* DHFR residues is well defined. Moreover, none of the active site residues of the model have geometric, conformational or energetic problems.

3.4. Molecular dynamics simulations of the drug-enzyme complexes

The modeled *Pf* DHFR structures have 3827 atoms, including hydrogens. This large number of atoms makes ligand-enzyme molecular dynamics simulations (MDS) computationally uneconomical. Thus, modeling approximations were sought to scale down the *Pf* DHFRs to more manageable sizes. In this way, the analysis was restricted to those amino acid residues, which were close to their active-site regions. To accomplish this reducing procedure on the modeled enzymes, the pruning method as proposed by Tokarski and Hopfinger [62], was followed. Fig. 5 shows a schematic representation of the used geometry for determining the enzyme model sizes.

Firstly, both drugs Pyr and Cyc were docked into the active site of the wild- and mutant-type *Pf* DHFRs. Thus, four enzyme-drug complexes (wild-type *Pf* DHFR-Pyr, mutant-type *Pf* DHFR-Pyr, wild-type *Pf* DHFR-Cyc, mutant-type *Pf* DHFR-Cyc) were obtained. Three different reduced-size enzyme models of each type of *Pf* DHFR were modeled in order to examine how the size of the enzyme structure could be reduced without losing information regarding the binding process. These models were created by pruning away all residues at a distance greater than 8, 10 and 12 Å from any atom of the bound drug, but if at least one non-hydrogen atom of these residues was found within the spherical cutoff, then that entire residue was included in the models. The pruning operation resulted in a model that is formed by a number of unconnected peptide fragments. The number of fragments in the enzyme models was kept to a minimum by not 'cutting' those fragments separated by less than or equal to four residues in the original *Pf* DHFR homology-model sequences. This approach was followed in order to retain the local geometric integrity of the enzyme model during the pruning process [62].

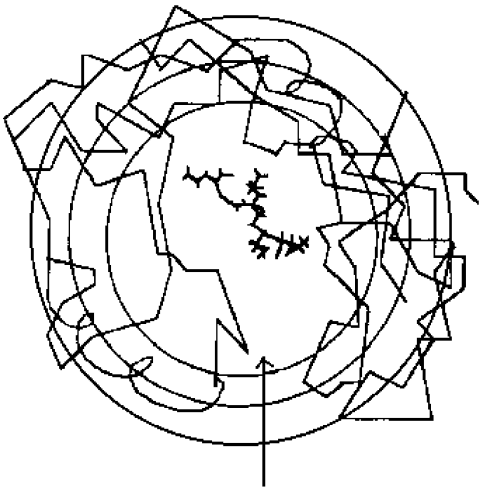

Fig. 5. Schematic representation of the used geometry for determining the enzyme models size. A ligand is docked into the active site. Three possible cutoffs are shown [62].

It was necessary to apply a constraint to each main-chain atom in the pruned enzyme models to 'fix' their positions in space and, consequently, to maintain the structural integrity of the models.

Thus, due of the exclusion of the rest of the enzyme, for each main-chain of atoms we assigned a fictitious mass of 5 kDa to serve as 'momentum reservoirs' and prevent significant departures from the model geometry due to the exclusion of the rest of the enzyme. The use of fictitious masses is virtually the same as the use of Cartesian constraints, particularly when the masses are chosen because of their very high values [62].

After a MDS of 2 ps at 310 K, the size of the enzyme models were selected based on a combination of geometric stability and the variance of the drug-enzyme interaction energy for the model radii (8, 10 and 12 Å). During this simulation, we used a non-bonded cutoff of 15 Å and a dielectric constant of 3.5. In this study, to compute non-scaled energy terms, all energy minimizations and MDS used a force field in which all parameters of the AMBER program [40–42] were adopted into a MM2 force field [63] potential function representation. Missing force field parameters (torsional, bonding stretching and bond angle bending) were taken and adjusted from the set proposed by Hopfinger [64] and the MM2 force field [63]. The 'combining' of AMBER and MM2 parameters is accomplished by linear scaling. The most similar set of atoms to those of the missing AMBER parameters is identified for a parameter that has both AMBER and MM2 values. The unknown AMBER parameter value is then scaled against the known MM2 value in the same ratio as the parameter having both AMBER and MM2 values. Energy minimization and MDS were performed using the MOLSIM [65] program.

The RMS fit of the lowest energy 8, 10 and 12 Å radii models found in MDS was 1.80, 1.60 and 1.94 Å, respectively, compared to the equivalent part of the original models. The total drug-enzyme interaction energies for the 8, 10 and 12 Å models are 604.04, 230.85 and 304.03 kcal mol^{-1}, respectively. Thus, for the subsequent simulations, the model size of 10 Å was selected for both the wild and the mutant types *Pf* DHFR homology-models.

The binding simulation was done, for each of the four pruned drug-enzyme models of 10 Å, by an MDS of 20 ps, using time steps of 0.5 fs and a relaxation time τ of 0.001 ps on the drug-enzyme complex models. The used dielectric constant was 3.5. During the simulation, the temperature was kept constant at 310 K by coupling each system to a constant temperature bath according to the method of Berendsen [66]. The total number of steps for each simulation was 40 000, and a conformation was taken at each 40 steps, generating 1000 conformational states. The lowest energy conformation of the *Pf* DHFR active site was taken for each modeled enzyme: wild-type enzyme-Pyr; mutant-type enzyme-Pyr; wild-type enzyme-Cyc; and mutant-type enzyme-Cyc complexes.

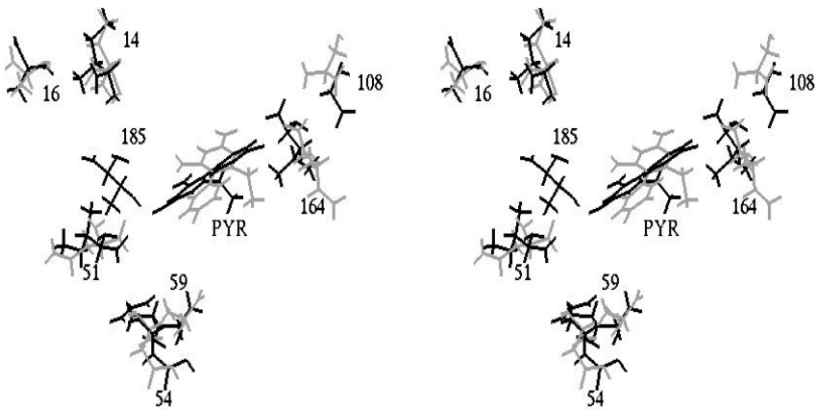

Fig. 6. Superposition of the active sites for both the wild- and mutant-type *Pf* DHFR with the docked inhibitor Pyr. The wild-type active site *Pf* DHFR-Pyr complex is shown in lighter color, the mutant-type *Pf* DHFR-Pyr complex is shown in darker color.

Fig. 6 shows the superposition between the active sites for both the wild- and mutant-type *Pf* DHFR with the inhibitor Pyr docked inside. Fig. 7 shows the superposition of the active sites, for both the wild- and mutant-type *Pf* DHFR, to the inhibitor Cyc docked inside. In both figures, the wild-type active site enzyme-inhibitor complexes are shown in a lighter color, whereas the corresponding mutant-type enzyme-inhibitor complexes are shown in a darker color.

Fig. 6 and Fig. 7 make possible to hypothesize an explanation for the resistance found to the mutant-type *Pf* DHFR enzyme. Steric hindrance seems to be the main cause for inhibition resistance regarding both drugs Pyr and Cyc.

Based on the analysis of Fig. 6 and Fig. 7, mutation at residue 164 (Ile → Leu) causes an obvious modification of the shape of the binding cavity around the drug. The leucine side chain is bulky and wider than the isoleucine side chain. From Figs. 6 and 7 it can be seem that the drugs are extremely close to one of the methyl groups of the leucine residue in the complexes with the mutant enzyme.

The residue at position 108 (Ser/Asn), which is further away from the inhibitor binding site, may play a role in the process of admission of the drugs to the site. It should also be an important component of the hydrophobic pocket enclosing the pyrimidine ring of the inhibitors. The participation of the mutation on residue 108 (Ser → Asn) in the resistance process is not completely clear in our model, however, it may cause some hindrance to the dynamical process of admission and accommodation of the inhibitors to the active site. The greater size of Asn as compared to Ser and the difference in polarity between these two residues could lead to a more difficult approximation of the drugs to the active site of the mutated enzyme. Also, because both residues 108 (Asn) and 164 (Leu) are close to each other, they could act in synergy regarding this effect.

As in the work of Rastelli [21], the participation of the mutation on residue 51 (Asn → Ile) is not evident. The role of the mutation on residue 59 (Cys → Arg) is also unclear but we believe that it is possible that the positive charge of the Arg residue in the mutation may lead to some repulsion of the inhibitors if they interact as their protonated forms. Apparently, the remaining residues of the active site Ile-14, Ala-16, Asp-54 and Thr-185, do not contribute significantly to the resistance mechanism. Regarding this, it should be observed that, in Fig. 6, there is a false perception regarding the position of Thr-185, which seems to be close to Pyr. In fact, this residue is far from the inhibitor, back inside the sheet plane.

4. Conclusion

Three-dimensional-homology models of a wild-type and a specific mutant-type (Asn-51 → Ile-51, Cys-59 → Arg-59, Ser-108 → Asn-108 and Ile-164 → Leu-164) of *P. falciparum* DHFR-domain were built based on pairwise alignment

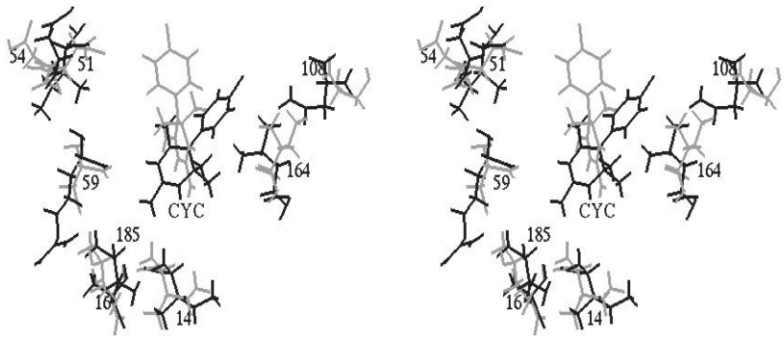

Fig. 7. Superposition of the active sites for both the wild- and mutant-type *Pf* DHFR with the docked inhibitor Cyc. The wild-type active site *Pf* DHFR-Cyc complex is shown in a lighter color, the mutant-type *Pf* DHFR-Cyc complex is shown in a darker color.

between the amino acid sequences of *P. falciparum* [11] and chicken liver [25] DHFRs. These models were successfully validated and were used to hypothesize an explanation of the resistance mechanism caused by specific point mutations. The interactions between both inhibitors Pyr and Cyc were evaluated and, according to the results, a 'steric constraint' hypothesis for the resistance was proposed. The models of the active site of the enzymes gave us a clear view of the importance of residue mutations regarding resistance mechanisms. We believe that these models contribute to a better understanding of the resistance mechanism and that they could be useful in the development of new potential antimalarial drugs.

Acknowledgements

We are grateful to Dr Geoffrey J. Barton (University of Oxford, UK) for the concession of an academic license for the Multalign program, to Dr Anton J. Hopfinger (The University of Illinois at Chicago, USA) for the use of the MOLSIM program, to Dr Thomas E. Wellems (National Institute of Health, USA) for information about the resistant strains of *P. falciparum* and to Ms Carlota da Cunha Parreira for revision of the text. We would also like to thank the Brazilian agencies, CNPq, FAPERJ and CAPES, for financial support.

References

[1] The World Health Organization Report, WHO Publications, Geneva, 1997.
[2] W. Peters, Drug resistance in malaria parasites of animals and man, Adv. Parasitol. 41 (1998) 1–62.
[3] S.J. Foote, A.F. Cowman, The mode of action and the mechanism of resistance to antimalarial drugs, Acta Tropica 56 (1994) 157–171.
[4] P. Newton, N. White, Malaria: new developments in treatment and prevention, Annu. Rev. Med. 50 (1999) 179–192.
[5] N.J. White, P.L. Olliaro, Strategies for the prevention of antimalarial drug resistance: rationale for combination chemotherapy for malaria, Parasitol. Today 12 (1996) 399–401.
[6] I.S. Soares, M.M. Rodrigues, Malaria vaccine: roadblocks and possible solutions, Braz. J. Med. Biol. Res. 31 (1998) 317–332.
[7] R.L. Blakley, Folates and pterinsin: R.L. Blakley, S.J. Benkovic (Eds.), Dihydrofolate Reductase, 1, John Wiley and Sons, New York, 1984, p. 191.
[8] K.A. Brown, J. Kraut, Exploring the molecular mechanism of dihydrofolate reductase, Faraday Discuss. 93 (1992) 217–224.
[9] J. Kraut, D.A. Matthews, Biological macromolecules and assembliesin: F. Jurnak, A. McPherson (Eds.), Dihydrofolate Reductase, 3, John Wiley and Sons, New York, 1987, p. 1.
[10] G.P. Miller, S.J. Benkovic, Stretching exercises: flexibility in dihydrofolate reductase catalysis, Chem. Biol. 5 (1998) R105–R113.
[11] D.J. Bzik, W. Li, T. Horii, J. Inselburg, Molecular cloning and sequence analysis of the *Plasmodium falciparum* dihydrofolate reductase-thymidylate synthase gene, Proc. Natl. Acad. Sci. USA 84 (1987) 8360–8364.
[12] D.S. Peterson, D. Walliker, T.E. Wellems, Evidence that a point mutant in dihydrofolate reductase-thymidylate synthase confers resistance to pyrimethamine in *falciparum* malaria, Proc. Natl. Acad. Sci. USA 85 (1988) 9114–9118.
[13] A.F. Cowman, M.J. Morry, B.A. Biggs, G.A.M. Cross, S.J. Fotte, Amino acid changes linked to pyrimethamine resistance in the dihydrofolate reductase-thymidylate synthase gene of *Plasmodium falciparum*, Proc. Natl. Acad. Sci. USA 85 (1988) 9109–9113.
[14] S. Thaithong, S.-W. Chan, S. Songsomboon et al., Pyrimethamine resistant mutations in *Plasmodium falciparum*, Mol. Biochem. Parasitol. 52 (1992) 149–158.
[15] J.W. Zolg, J.R. Plitt, G.X. Chen, S. Palmer, Point mutation in the dihydrofolate reductase-thymidylate synthase gene as the molecular basis for pyrimethamine resistance in *Plasmodium falciparum*, Mol. Biochem. Parasitol. 36 (1989) 253–262.
[16] J.E. Hyde, Point mutations and pyrimethamine resistance in *Plasmodium falciparum*, Parasitol. Today 5 (1989) 252–255.
[17] S.J. Foote, D. Galatis, A.F. Cowman, Amino acids in the dihydrofolate reductase-thymidylate synthase gene of *Plasmodium falciparum* involved in cycloguanil resistance differ from those involved in pyrimethamine resistance, Proc. Natl. Acad. Sci. USA 87 (1990) 3014–3017.
[18] L.K. Basco, P.E. de Pécoulas, C.M. Wilson, J. Le Bras, A. Mazabraud, Point mutations in the dihydrofolate reductase-thymidylate synthase gene and pyrimethamine and cycloguanil resistance in *Plasmodium falciparum*, Mol. Biochem. Parasitol. 69 (1995) 135–138.
[19] D.S. Peterson, W.K. Milhous, T.E. Wellems, Molecular basis of differential resistance to cycloguanil and pyrimethamine in *Plasmodium falciparum* malaria, Proc. Natl. Acad. Sci. USA. 87 (1990) 3018–3022.

[20] T. Lemck, I.T. Christensen, F.S. Jørgensen, Towards an understanding of drug resistance in malaria: three-dimensional structure of *Plasmodium falciparum* dihydrofolate reductase by homology building, Bioorg. Med. Chem. 7 (1998) 1003–1011.

[21] G. Rastelli, W. Sirawaraporn, P. Sompornpisut et al., Interaction of pyrimethamine, cycloguanil, WR99210 and their analogues with *Plasmodium falciparum* dihydrofolate reductase: structural basis of antifolate resistance, Bioorg. Med. Chem. 8 (2000) 1117–1128.

[22] C. Oefner, A. D'arcy, F.K. Winkler, Crystal structure of human dihydrofolate reductase complexed with folate, Eur. J. Biochem. 174 (1988) 377–385.

[23] M.R. Sawaya, J. Kraut, Loop and subdomain movements in the mechanism of *Escherichia coli* dihydrofolate reductase: crystallographic evidence, Biochemistry 36 (1997) 586–603.

[24] J.T. Bolin, D.J. Filman, D.A. Matthews, R.C. Hamlin, J. Kraut, Crystal structures of *Escherichia coli* and *Lactobacillus casei* dihydrofolate reductase refined at 1.7 Å resolution. 1. General features and binding of methotrexate, J. Biol. Chem. 257 (1982) 3650–3662.

[25] M.A. McTigue, J.F. Davies II, B.T. Kaufman, J. Kraut, Crystal structure of chicken liver dihydrofolate reductase complexed with $NADP^+$ and biopterin, Biochemistry 31 (1992) 7264–7273.

[26] J.N. Champness, A. Achari, S.P. Ballantine, P.K. Bryant, C.J. Delves, D.K. Stammers, Structure of *Pneumocystis carinii* dihydrofolate reductase to 1.9 Å resolution, Structure 2 (1994) 915–924.

[27] F.C. Bernstein, T.F. Koetzle, G.J. Williams et al., The protein data bank. A computer-based archival file for macromolecular structures, J. Mol. Biol. 112 (1977) 535–542.

[28] H.M. Berman, J. Westbrook, Z. Feng et al., The protein data bank, Nucl. Acids Res. 28 (2000) 235–242.

[29] G.J. Barton, Protein multiple sequence alignment and flexible pattern matching, Methods Enzymol. 183 (1990) 403–428.

[30] N. Guex, M.C. Peitsch, SWISS-MODEL and Swiss-PdbViewer: an environment for comparative protein modeling, Electrophoresis 18 (1997) 2714–2723.

[31] M.C. Peitsch, Protein modeling by e-mail. From amino acid sequence to protein structure: a free one-hour service, BioTechnology 13 (1995) 658–660.

[32] M.C. Peitsch, Biochem ProMod and SWISS-MODEL: internet-based tools for automated comparative protein modeling, Soc. Trans. 24 (1996) 274–279.

[33] R.A. Laskowski, M.W. MacArthur, D.S. Moss, J.M. Thornton, Pro-check: a program to check the stereochemical quality of protein structures, J. Appl. Cryst. 26 (1993) 283–291.

[34] G. Vriend, WHAT IF: a molecular modeling and drug design program, J. Mol. Graph. 8 (1990) 52–56.

[35] (http://biotech.embl-heidelberg.de:8400/)

[36] J.F. Cortese, C.V. Plowe, Antifolate resistance due to new and known *Plasmodium falciparum* dihydrofolate reductase mutations expressed in yeast, Mol. Biochem. Parasitol. 94 (1998) 205–214.

[37] W. Sirawaraporn, S. Yongkiettrakul, R. Sirawaraporn, Y. Yuthavong, D.V. Santi, Exp. *Plasmodium falciparum*: asparagine mutant at residue 108 of dihydrofolate reductase is an optimal antifolate-resistant single mutant, Parasitology 87 (1997) 245–252.

[38] J.C. Reeder, K.H. Rieckmann, B. Genton, K. Lorry, B. Wines, A.F. Cowman, Point mutations in the dihydrofolate reductase and dihydropteroate synthase gene and in vivo susceptibility to pyrimethamine and cycloguanil of *Plasmodium falciparum* isolates from Papua New Guinea, Am. J. Trop. Med. Hyg. 55 (1996) 209–213.

[39] D.S. Peterson, S.M. di Santi, M. Povoa, V.S. Calvosa, V.E. do Rosario, T.E. Wellems, Prevalence of the dihydrofolate reductase Asn-108 mutation as the basis for pyrimethamine-resistant falciparum malaria in the Brazilian Amazon, Am. J. Trop. Med. Hyg. 45 (1991) 492–497.

[40] S.J. Weiner, P.A. Kollman, D.T. Nguyen, D.A. Case, An all atom force field for simulations of proteins and nucleic acids, J. Comput. Chem. 7 (1986) 230–252.

[41] S.J. Weiner, P.A. Kollman, AMBER. Assisted model building with energy refinement. A general program for modeling molecules and their interactions, J. Comput. Chem. 2 (1981) 287–303.

[42] S.J. Weiner, P.A. Kollman, D.A. Case et al., A new force field for molecular mechanical simulation of nucleic acids and proteins, J. Am. Chem. Soc. 106 (1984) 765–784.

[43] Molecular Simulations Inc., 9685 Scranton Road, San Diego, CA 92121-3752, USA.

[44] A.R. Leach, Molecular Modeling: Principles and Applications, Addison-Wesley, Essex, 1996.

[45] F. Jensen, An Introduction to Computational Chemistry, John Wiley and Sons, Chichester, 1999.

[46] G.N. Ramachandran, V. Sasisekharan, Conformation of polypeptides and proteins, Adv. Prot. Chem. 23 (1968) 283–437.

[47] K.W. Volz, D.A. Matthews, R.A. Alden et al., Crystal structure of avian dihydrofolate reductase containing phenyltriazine and NADPH, J. Biol. Chem. 257 (1982) 2528–2536.

[48] S. Lifson, A. Warshel, Consistent force field for calculations of conformations, vibrational spectra, and enthalpies of cycloalkane and *n*-alkane molecules, J. Chem. Phys. 49 (1968) 5116–5129.

[49] A. Warshel, S. Lifson, Consistent force field calculations. II. Crystal structures, sublimation energies, molecular and lattice vibrations, molecular conformations, and enthalpy of alkanes, J. Chem. Phys. 53 (1970) 582–594.

[50] A.T. Hagler, P.S. Stern, S. Lifson, S. Ariel, Urey–Bradley force field, valence force-field, and ab initio study of

intramolecular forces in tri-*tert*-butylmethane and isobutane, J. Am. Chem. Soc. 101 (1979) 813–819.
[51] S. Lifson, A.T. Hagler, P. Dauber, Consistent force field studies of intermolecular forces in hydrogen bonded crystals. 1. Carboxilic acids, amides, and the C=O...H hydrogen bonds, J. Am. Chem. Soc. 101 (1979) 5111–5120.
[52] A.T. Hagler, S. Lifson, P. Dauber, Consistent force field studies of intermolecular forces in hydrogen bonded crystals. II.A benchmark for the objective comparison of alternative force fields, J. Am. Chem. Soc. 101 (1979) 5122–5130.
[53] A.T. Hagler, P. Dauber, S. Lifson, Consistent force field studies of intermolecular forces in hydrogen bonded crystals. III. The C=O...H–O hydrogen bond on the analysis of the energetics and packing of carboxylic acids, J. Am. Chem. Soc. 101 (1979) 5131–5141.
[54] S. Lifson, P.S. Stern, Born–Oppenheimer energy surfaces of similar molecules. Interrelations between bond lengths, bond angles, and frequencies of normal vibrations in alkanes, J. Chem. Phys. 77 (1982) 4542–4550.
[55] J.M. Blaney, C. Hansch, C. Silipo, A. Vittoria, Structure-activity relationships of dihydrofolate reductase inhibitors, Chem. Rev. 84 (1984) 333–407.
[56] D.J. Baker, C.R. Beddell, J.N. Champness, P.J. Goodford, F.E. Norringhton, B. Roth, D.K. Stammers, Chemistry and biology of pteridines: pteridines and folic acid derivativesin: A. Blair (Ed.), X-Ray Studies of Binding of Trimethoprim, Methotrexate, Pyrimethamine and Two Trimethoprim Analogues to Bacterial Dihydrofolate Reductase, Walter de Gruyter, Berlin and New York, 1983, p. 545.
[57] D.A. Matthews, J.T. Bolin, J.M. Burridge et al., Refined crystal structures of *Escherichia coli* and chicken liver dihydrofolate reductase containing bound trimethoprim, J. Biol. Chem. 260 (1985) 381–391.
[58] D.A. Matthews, J.T. Bolin, J.M. Burridge, D.J. Filman, K.W. Volz, J. Kraut, Dihydrofolate reductase. The stereochemistry of inhibitor selectivity, J. Biol. Chem. 260 (1985) 392–399.
[59] J.F. Davies II, T.J. Delcamp, N.J. Prendergast, V.A. Ashford, J.H. Freisheim, J. Kraut, Crystal structures of recombinant human dihydrofolate reductase complexed with folate and 5-deazafolate, Biochemistry 29 (1990) 9467–9479.
[60] W. Sirawaraporn, Dihydrofolate reductase and antifolate resistance in malaria, Drug Res. Updates 1 (1998) 397–406.
[61] D.C. Warhurst, Antimalarial drug discovery: development of inhibitors of dihydrofolate reductase active in drug resistance, Drug Disc. Today 3 (1998) 538–546.
[62] J.S. Tokarski, A.J. Hopfinger, Constructing protein models for ligand-receptor binding thermodynamics simulations: an application to a set of peptidometic renin inhibitors, J. Chem. Inf. Comput. Sci. 37 (1997) 779–791.
[63] N.L. Allinger, Conformational analysis. 130. MM2. A hydrocarbon force field utilizing V_1 and V_2 torsional terms, J. Am. Chem. Soc. 99 (1977) 8127–8134.
[64] A.J. Hopfinger, Conformational Properties of Macromolecules, Academic Press, New York, 1973, p. 38.
[65] D.C. Doherty, MOLSIM User Guide, The Chem21 Group, 1780 Wilson Dr., Lake Forest, IL, 60045, 1994.
[66] H.J.C. Berendsen, J.P.M. Postman, W.F. van Gunsteren, A. Di Nola, J.R. Haak, Molecular dynamics with coupling to an external bath, J. Chem. Phys. 81 (1984) 3684–3690.